Al-Azhar Bulletin of Science Vol. 31, No. 2, (December) 2020, pp. 11-19

GAS TYPE ROLE ON THE DYNAMICS OF CHANNEL SPARK PULSED ELECTRON DEPOSITION SYSTEM

A.S.A. Abdo[1], M.A.I.Elgarhy[1,2*], A. Abouelsayed[3] ,U.M. Rashed[1], and S. E. Hassaballa[1,4]

1 *Department of Physics, Faculty of Science, (Boys) Al-Azhar University, Cairo, Egypt.*
2 *Department of Nuclear Engineering, Seoul National University, Seoul, Korea.*
3 *Spectroscopy Department, Physics Division, National Research Centre, Giza, Egypt.*
4 *Department of Physics Faculty of Science, Islamic University of Madinah, Medina, Saudi Arabia.*
* Corresponding Author: elgarhy@azhar.edu.eg, elgarhy@snu.ac.kr

ABSTRACT

In this paper, the effect of feeding gas type on the dynamics of channel spark pulsed electron deposition system is investigated. Electrical, magnetic, and optical characterisations of the system were measured for different feeding gases, oxygen (O_2), nitrogen (N_2), and argon (Ar). The discharge current for each gas type was measured with maximum value of 1189 A for O_2 at -13 kV applied voltage. The discharge current and voltage waveforms were simulated by LRC circuit theory. Effect of gas pressure on the maximum discharge current and total inductance was also investigated. The beam current investigated by faraday cup and reached maximum electron beam current of 136 A for O_2 gas. Two magnetic pickup coils were employed for the measurements of beam kinetic dynamics and the measured beam speed was around 0.4×10^6 m/sec. Electron beam plasma density was calculated from faraday cup and magnetic coils signals and found to be 1.96×10^{20} m^{-3}. Optical emission spectra were also measured to identify reactive species and its role in electron beam interaction with graphite target for thin film deposition application. The ability of using the system for thin film deposition is demonstrated by depositing amorphous hydrogenated carbon (a-C:H) films over silicon substrates.

Keywords: Channel spark, Pulsed electron deposition, Thin film deposition, Amorphous hydrogenated carbon.

1. INTRODUCTION

Pulsed deposition devices allow exceptional material deposition technology. The short pulse length, on the order of about 10-100 ns, results in high power density at the target material surface. This leads to generation of rapid heating process and formation of a plasma plume. On the other hand, commercial production of pulsed deposition devices on large scale is limited due to high costs which decrease the efficiency of such techniques. Thus, it is essential to find a technology permitting both high throughput deposition characteristics and low running costs. These criteria can be realised by pulsed electron deposition (PED). Channel spark pulsed electron beam system is a promising technique for thin film deposition. A comparative study among pulsed intense electron beam systems showed that, Channel spark system has higher beam intensities and longer pulse lengths at low voltages than other systems [1-3].

The electron beam generated in the channel spark device is the most suitable pulsed electron beam source for material processing. Channel spark is a kind of pulsed electron deposition (PED) devices that recently has attracted considerations in many fields of materials processing. This is mainly due to the higher energy transfer to the target material as well as low running costs when compared to pulsed laser deposition (PLD) [4]. Ideally, pulsed electron beams are generated in transient hollow cathode discharges employing low gas pressures (10^{-3}–10^{-1} mbar) and discharge voltage on the order of few kV up to tens of kV [5,6].

Afterwards, a novel PED system called Channel Spark was designed allowing higher conversion efficiency of electrical energy stored. This conversion efficiency reached 30% compared to only 4% of pseudo spark discharge. Despite its simplicity, only with a suitable device design, one can attain beam parameters suitable for PED (e.g., electron beam current, energy, and plasma density) [7,8]

Practically, the focused electron beam extracted by the plasma passes through a tiny cathode hole and is guided into 4-6 mm diameter tube to the target material. Normally this tube is made of glass or alumina or any other dielectric material. The high potential difference applied between the hollow cathode and the target holder (ground) results in an acceleration of the electron beam. To store the electrical energy high voltage ceramic capacitors are employed. These capacitors can deliver an energy of about 3-5 J/pulse. An external triggering circuit is used to initiate the discharge. Because of the focusing of the beam (several mm^2 in area), high current density in the beam can be achieved (about 10^6 A/cm^2). This leads to very high-power density (up to 10^9 W/cm^2) onto the surface of the target material. Subsequently, the energy is absorbed by the surface and a fast rise of the temperature occurs, producing a rapid evaporation of the material and the formation of the plume composed of ablated material. Commonly, in high pulsed energy ablation, the plasma plume produced at the target surface expands in the direction of the maximum pressure incline [9, 10].

PED is a well-established technology to fabricate thin films for photovoltaic, superconductor, and optoelectronic applications [11, 12]. PED technology belongs to the family of the channel spark discharges, in which a target material is ablated by the local heating induced by an accelerated electron beam. At the very beginning, this technique was mainly employed for the deposition of both inorganic, i.e., superconductive $MBa_2Cu_3O_{7-x,}$ and organic, i.e., polytetrafluoroethylene (PTFE), thin films. The deposition applications of the technique expanded in the past years to include for example, biomedical materials, $CuInGaSe_2$ Solar Cells, In_2O_3 nano-films, $LaMnO_3$ thin Films, Poly (ethylene-co-vinyl acetate) films and nanostructured Ag thin films [13-17].

In this paper, the role of the gas type in the dynamics of the electron beam pulse system of the spark channel and the possibility of using the system for thin film deposition of carbon thin films is studied.

EXPERIMENTAL SETUP

Experimental setup for our channel spark Pulsed electron deposition system can be found in details in our previous publication [1]. The difference here is using of a commercial spark plug as triggering source for plasma generation. Figure 1 shows the experimental arrangement and the electrical circuit for coupling the negative high voltage signals to the device. The length of channel tube is 15 cm and the distance between hollow cathode and anode chamber is 5.5 cm. The 10 KΩ resistor was used to hold the discharge voltage at the main discharge tube and to ensure that the discharge is occurring first at this tube. Besides this resistor is (DC) blocking the capacitor discharge before the glow discharge is established at the main tube. O_2, N_2, and Ar gases in pressure range of 20–30 mTorr were employed as discharge gases. The applied voltage is varied between 9 and 13 kV with an external capacitance of 21.6 nF. Pearson coil and high voltage probe were used to monitor the discharge current and the voltage. Additionally, to investigate electron beam current characteristics a faraday cup was employed. An optical emission spectrometer (Ocean Optics USB4000 Spectrometer) was employed to monitor the reactive species during plume formation after bombardment of electron beam with the target (graphite).

EXPERIMENTAL RESULTS

1. Electric characterization

To study electrical characteristics of the system, the discharge current and voltage for O2, Ar and N_2 as working gases were measured at different discharge voltage, pressure and capacitance. Figure 2 a, b, c shows a typical

discharge current and voltage waveforms for O2, Ar and N_2 respectively at pressure 20 mTorr and applied voltage -13 kV. When plasma reaches the cathode opening, capacitor starts discharging, so, the current quickly increases and the voltage drops down. In the hollow cathode discharge, the electrons have energy in same range of the accelerating voltage [18]. Note the N_2 discharge current is positive to reverse the Rogowski direction.

Figure 2 shows that, the current reached maximum value at 1110 A after a period of ~ 466 nsec for Ar ,~ 1189 A after a period of ~ 343 nsec for O_2, and ~ 910 A after a period of ~ 387 nsec for N_2. The voltage started from (-13 kV) then the voltage falls to zero after 400 nsec.

Oscillations in the discharge current waveform were thought to be due to the

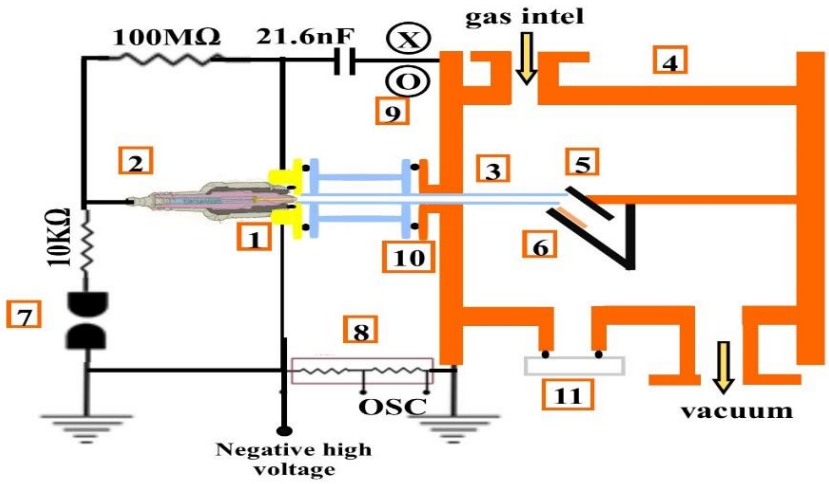

Fig.1 Sketch of the used system, (1) hollow cathode, (2) spark plug, (3) acceleration tube, (4) anode deposition chamber, (5) graphite target, (6) substrate, (7) spark gap switch, (8) potential divider, (9) Pearson coil, (10) O-ring, and (11) glass window.

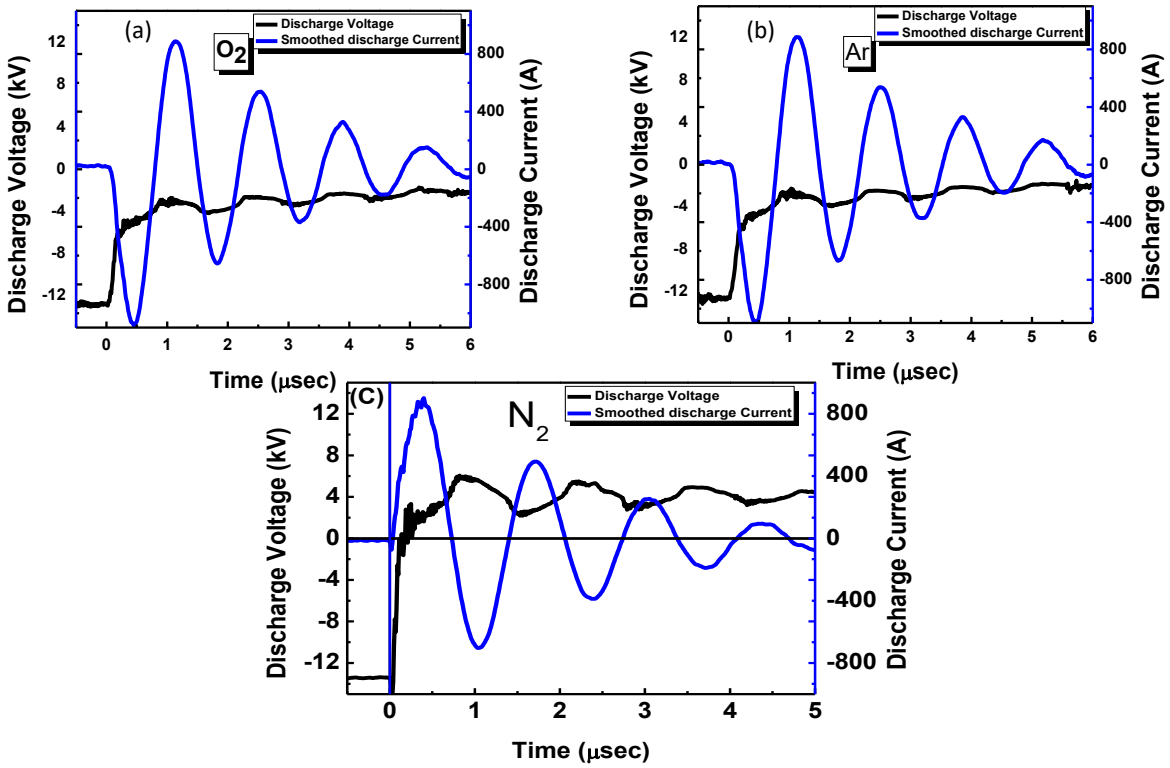

Fig. 2 (a, b, c): Discharge voltage and current signals for O_2, Ar, and N_2 gases respectively at 13 kV.

development of high-conductivity plasma channel between the ground electrode and the hollow cathode [19]. Current and voltage waveforms simulation were performed based on LCR circuit theory and shown in figure (3) for N_2 plasma. It should be noted that this simulation is only performed after the discharge of the capacitor on the beam acceleration section which can be simply modeled as a capacitor discharging in series with coil and resistor.

Based on this circuit theory current equation can be written as:

$$I = I_0 e^{-\alpha t} \cos(\omega t)$$

Where, $\omega = \sqrt{\frac{1}{LC} - \left(\frac{R}{L}\right)^2}$ is an angular frequency and $\alpha = \frac{R}{2}\sqrt{\frac{C}{L}}$ is the damping factor.

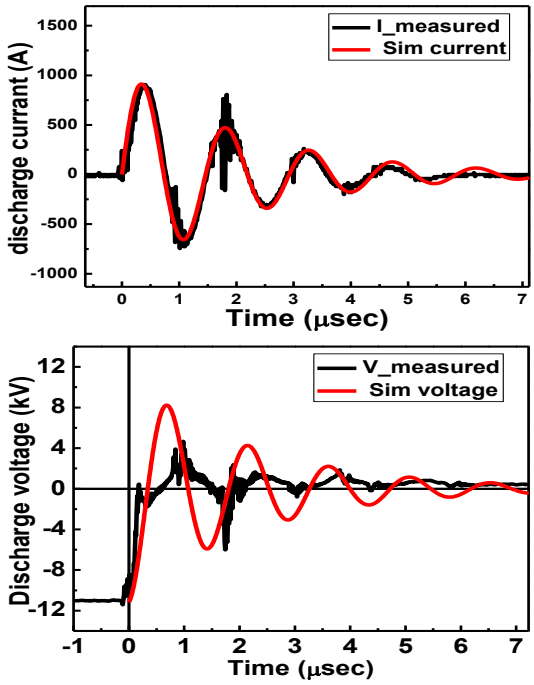

Fig. 3 Voltage and current waveforms simulations.

It can be noticed from fig. 3 that, there is a good match between measured and simulated current waveforms. On the other hand, there is a mismatching between measured and simulated voltage waveforms due to the noise that picked up by the potential divider of bad isolation.

Variation of the maximum discharge current with applied voltage was calculated and shown in fig. 4 It was found that, there is a slight difference in maximum discharge current when using O_2, Ar, and N_2. So, the discharge characteristics may be independent of gas type [20].

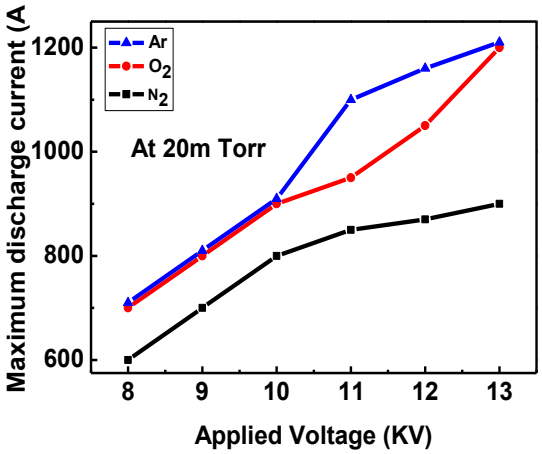

Fig.4: Dependence of maximum discharge current with the applied voltage for Ar, $O_2$and N_2.

Variations of the maximum discharge current and the total circuit inductance with operating gas pressure at varied discharge voltages for O_2 plasma were investigated and shown in fig. 5 (a, b) It is found that, with increase in both the pressure and discharge voltage the maximum discharge current increases. The maximum current was 1300 A at an applied voltage of -13 kV for Ar gas. On the other hand, because the device works in the left side of the Paschen curve, increasing the gas pressure leads to an increase in the maximum discharge current at a constant applied voltage [19]. By increasing the applied voltage more energy is pumped to the device, which results in an increase in the discharge current amplitude. The total inductance would be increased as both the pressure and the applied voltage decrease.

The rise in the pressure results in an increase in the plasma inductance, and consequently in a decrease in the periodic time of the current [10].

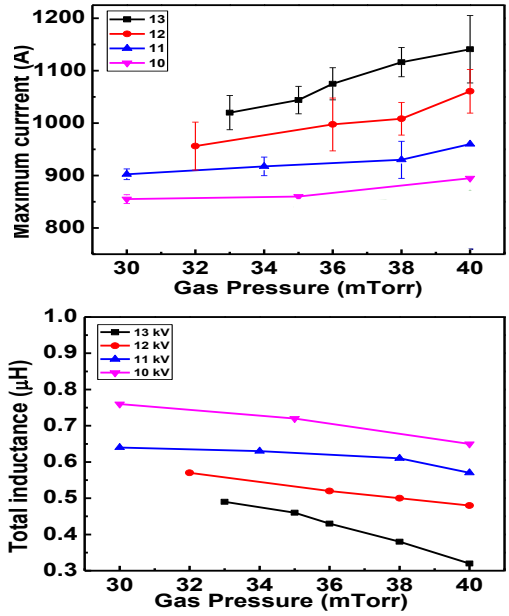

Fig.5: Dependence of maximum discharge current and total circuit inductance on gas pressure.

The electron beam current was measured by a faraday cup placed at 2 cm away from the end of the accelerating tube. Figure 6 shows a typical discharge current and electron beam current signals measured at -13 kV applied voltage, and 20 mTorr O_2 and Ar gas pressures. It was found that maximum electron current for O2 (136 A) is greater than that of Ar (95 A) at the same conditions of applied voltage 13 kV and external capacitance of 21.6 nF.

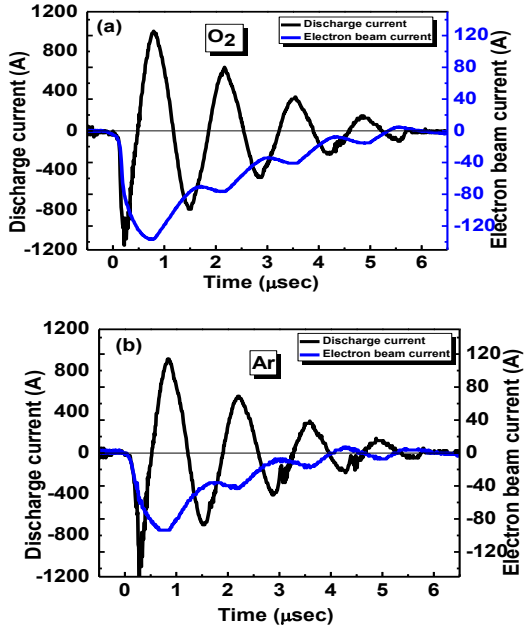

Fig. 6 (a,b): Electron beam current signals for O_2 and Ar respectively at 13 kV.

2. Magnetic characterization

Two identical coils of 5 turns wounded at the same directions were installed at the acceleration tube to measure the magnetic properties of the accelerated electron beam. By using pick up coils electron beam speed was measured using time of flight method [19]. Figure 7 shows the measured electron beam speed was found to be about 0.37985×10^6 m/sec and the corresponding value of beam kinetic energy was 4.1 eV. This value is greater than that obtained in our previous X-ray emission measurements which were less than 3 keV with efficiency of about 30% [1].

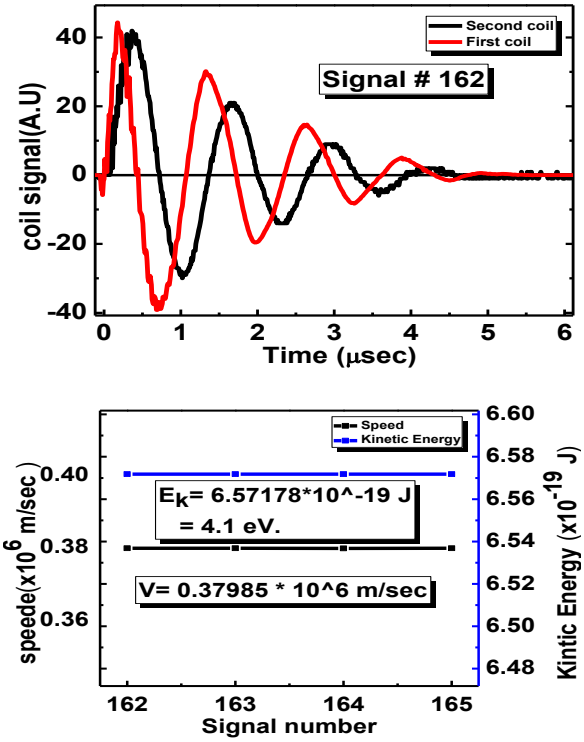

Fig. 7: Magnetic pickup coils signals and associated measured beam speed and beam energy.

Plasma density due to beam acceleration can be calculated from maximum beam current and beam speed. It was found to be around 1.96×10^{20} m^{-3}. As reported in [13], the current density J_{eff} of an electron beam is limited by the electron space-charge effect and is given by equation 1.

$$J_{eff} = (2.3\times10^{-6})V_a^{3/2}/d^2 \qquad \left(\frac{A}{m^2}\right) \qquad (1)$$

Where V_a is the acceleration voltage and d is the distance between the two electrodes.

3. Optical characterization

Optical emissions spectra resulting from the interaction of the beam with the target (graphite) in presence of Ar and O_2 gases at applied voltage of 13 kV, measured from near the target surface are presented in Fig. 8 (a, b).

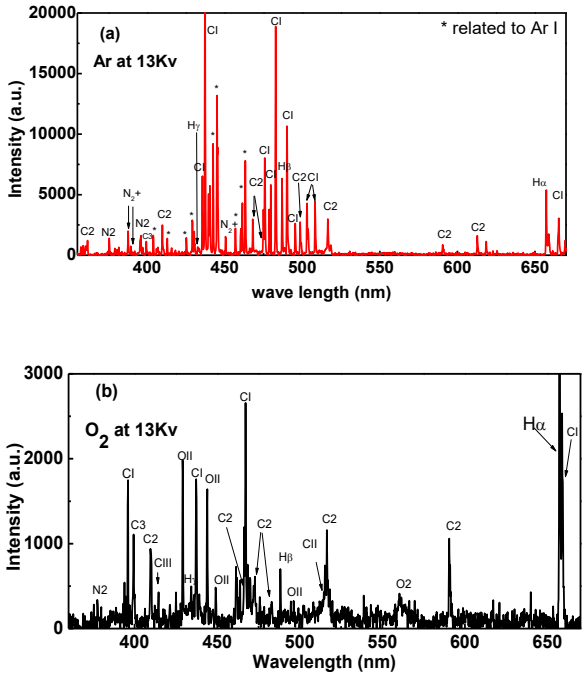

Fig. 8 (a, b) Emission spectra for Ar and O_2 respectively at 13 kV.

In figure 8 (a, b) we observe the formation of different ions like Ar^+, O^+, O^{++}, C^+, and C^{++} and different excited atoms and molecules like Ar, O_2, C_2, N_2, and H (α, β, γ). At the presence of the Ar gas (see figure 8a) the electron beam continued to collision with the Ar atoms along the path between the end of the acceleration tub and target surface this produced the Ar atoms and ions, similarly with the O_2 gas (see figure 8b).

Carbon species were produced from the collision of the electron beam with the target surface. The ions that were produced from the collision deposit onto the substrate and produce a-C thin film. Also, we observe the formation of different species of N_2 (ions and excited molecules). These products were produced from the collision of the electron beam with N_2; we attribute the presence of the N_2 to the base pressure. We also observe the formation of the H (α, β, γ). The source of the H_2 came from both the target material and the base pressure.

4. FTIR measurements

The a-C:H films deposited over silicon substrate at different accelerating voltages between 9 to 13 kV for two different gasses O_2 and Ar show polymeric characteristics. FTIR spectra of the deposited a-C:H films at different experimental conditions are shown in figure 9. The spectra have narrow and well resolved vibrational bands and allow water to diffuse into the material along columnar assemblies as observed by typical H_2O absorption bands around 1700 and 3250 cm^{-1}.

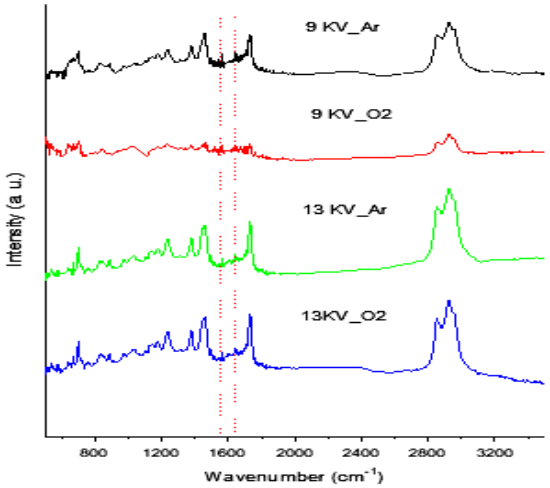

Fig. 9: FTIR spectra of the deposited a-C:H films at different experimental conditions.

As shown by fig. 9 one can find C-H deformation vibrations between 1300 to 1500 cm^{-1}, C=C stretching vibrations between 1500 and 1700 cm^{-1} from the carbon network, and C-H stretching vibrations around 3000 cm^{-1} [21-23].

The structure difference between the deposited films is due to difference in beam energy and current of Ar and O_2 as discussed before in the electrical characterization of the system. The films can be considered ta:C or a-C:H depending on the C-C sp^3 bonds are saturated with some C-H sigma bond or the sp^3 fraction is only related to pure C-C sigma bond. The last situation is mainly confirmed by the FTIR results as we will see later from fitting that some of C-C sp^3 bond are saturated with hydrogen atoms. Obviously, the shape and the total intensity of the peak are quite sensitive to

the film structure. Soft, polymerlike hydrocarbon layers are characterized by a well-structured, intense IR absorption band. The CH vibrational bands can be considered as fingerprint for the type of a-C:H film. The changes of the microstructure of the deposited films. For all deposited films, it is clear that the density of sp^3-CH_3, sp^3-CH_2, sp^3-CH groups, which contribute very strongly to the observed structure are very high while the density of sp^2-CH_x groups are very low. The infrared absorption cross sections (often also called dipole strength) for the latter groups, for the sp^2-related bands, is significantly lower than for the sp^3-CH_3 groups. In order to obtain both sp^2 and sp^3 fraction and hence know more information about the films structure synthesized at different condition we were performed quantitative analysis by fitting the IR spectra by Lorentzian as following:

$$e_2(\omega) = 2nk = \sum_j \frac{T_{8j}^2 \gamma j \omega}{(\omega_j^2 - \omega^2) + \gamma_j^2 \omega^2}$$

The optical constants in these equations are γj, Tsj and ωj damping, the oscillator strength, and the central frequency, respectively. Fig.9 show the IR spectra of the a-C:H films deposited at different conditions together with fitting curves and its component. It is clear from the fitting contributions the sp^3-CH_3, sp^3-CH_2, sp^3-CH groups stretching and bending modes recorded from films appeared with higher intensity as compared to sp^2-CH_x groups stretching modes which is related to the aromatic bonds (see Fig9). Furthermore, we have extracted the total area of both contributions sp^3-CH_x, and sp^2-CH_x groups for all films as shown in figure 10, which reflects the amount of sp^3 and sp^2 in the deposited films these values are listed in table1. In a-C:H samples the optical gap is related to the sp^3 content through the following formula.

$$Eg = 4.59\ x^2 - 0.561\ x + 0.539 \qquad (1)$$

In this equation x is the sp3 content, and Eg is the optical band gap. The relation between Eg and H content in the samples can be obtained through the following relation.

$$H = (Eg + 0.9)/9 \qquad (2)$$

The Eg, and H content estimated according to equation 1,2 are listed in table 1 for all deposited films.

Comparison between the structure of the films deposited for O_2 and Ar as feeding gasses at two different charging voltage of 9 and 13 kV is shown in Table 1.

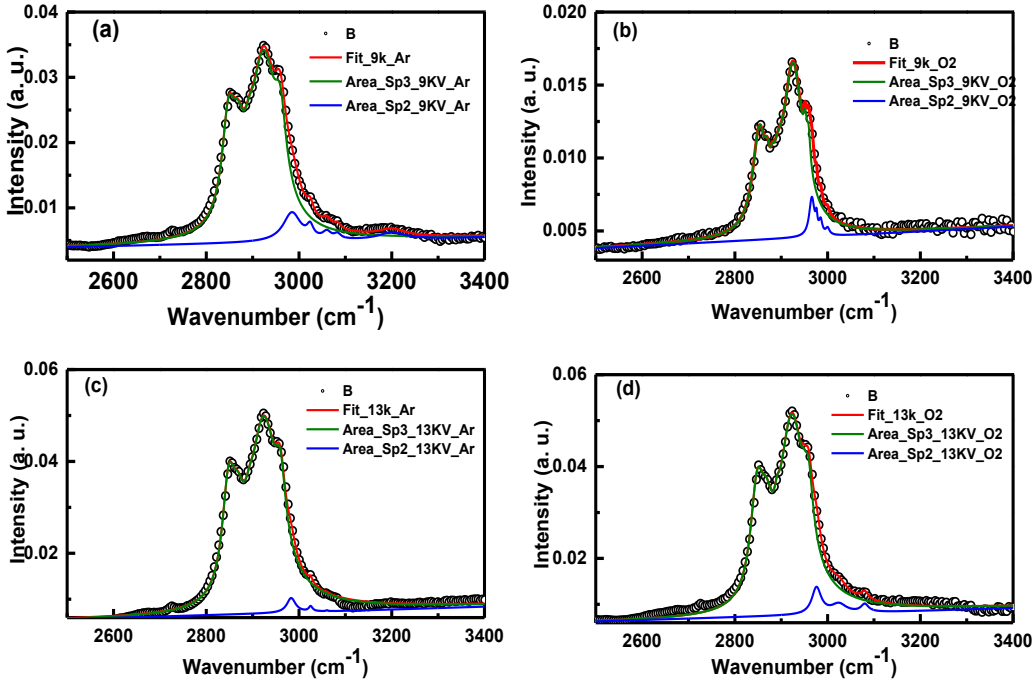

Fig. 10: Area estimation of sp^3 CHx and sp^2 CHx contributions of the deposited a-C:H films at different experimental conditions.

Table 1 comparison between the structures of the deposited films at different conditions.

Samples	SP3 %	SP2 %	Eg (eV)	H %
9kV_Ar	63.61775	36.38225	2.04041	32.67126
9kV_O_2	56.15942	43.84058	1.67214	28.57932
13kV_Ar	65.50758	34.49242	2.14184	33.7982
13kV_O_2	63.31512	36.68488	2.02448	32.49418

CONCLUSION

In this paper, the gas type role on the dynamics of channel spark pulsed electron deposition system was studied. Electrical, magnetic, and emission properties of channel spark system were examined for oxygen, argon, and nitrogen gases. Discharge current and voltage waveforms are best described and simulated using LCR circuit theory. The discharge characteristics may be independent of gas type. With increase in both the pressure and the discharge voltage the maximum discharge current increases. The presence of carbon excited species in the optical emission spectra confirmed the interaction of the electron beam with the graphite target. The possibility of using the electron beam in the deposition of carbon thin films is demonstrated by the deposition of a-C:H thin films on silicon substrates as confirmed by FTIR measurements.

REFERENCES

[1] M. A. I. Elgarhy, S. E. Hassaballa, U. M. Rashed, M. M. ElSabbagh, H. M. Soliman and A. H. Saudy, 2015 , “Generation of a pulsed low-energy electron beam using the channel spark device”, Rev. Sci. Instrum. 86.

[2] E. Oks, “Plasma Cathode Electron Sources”, Germany: Wiley-VCH, 2006.

[3] K. F. E. Dewald, D. Hoffmann and A. Tauschwitz, "Pulsed intense electron beams produced in high voltage hollow cathode discharges: a comparative study ” , 2001, Pulsed Power Plasma Science 2001. 28th IEEE International Conference on Plasma Science and 13th IEEE International Pulsed Power Conference. Digest of Papers (Cat. No.01CH37251), Las Vegas, NV, USA, 2001.

[4] N. B. M. M. Nistor, “The Channel-Spark Discharge As A pulsed, Intense Electron And X-Ray Source”, 2008,Romanian Reports in Physics, vol. 60, pp. 615-626,.

[5] S. G. P. N. &. C. T. Ya. E. Krasik, 2007, “Pressure and electron energy measurements in a channel spark discharge ” ,Plasma Devices and Operations, vol. 15, pp. 107-114.

[6] D. Y. J. F. Y. E. K. P. N. a. C. T. S. Gleizer, 2009, “Electron beam and plasma modes of a channel spark discharge operation”, JOURNAL OF APPLIED PHYSICS, vol. 106, p. 073301.

[7] U.M.Rashed and T. M.A.Elgarhy, 2012, “Investigation of Ion Beams and X-Rays Emission from UNU-ICTP plasma focus. ”, Arab Journal of Nuclear Science and Applications, vol. 45, p. 3.

[8] Y. Nakagawa and H. Kawauchi, 2001 ,“Production of a pulsed high‐density electron beam by channel spark discharge”, Electrical engineering in Japan, vol. 134, pp. 10-18.

[9] C. A. Brau, I. L. Raybun, J. B. Dodge and F. M. Gilman, 1977, “Simple, pulsed, electron beam gun”, Rev. Sci. instum., vol. 48.

[10] E. Dewald, K. Frank, D. Hoffmann and A. Tausch, 2001, “ Pulsed Power Plasma Science”. 28th IEEE International Conference on Plasma Science and 13th IEEE International Pulsed Power Conference. Digest of Papers (Cat. No.01CH37251), vol. 2, pp. 1362

[11] Wan, R.; Yang, M.; Zhou, Q.; Zhang, Q. Transparent conductive indium zinc oxide films prepared by pulsed plasma deposition. *J. Vac. Sci. Technol. A* **2012**, *30*, 61508.

[12] Yang, M.; Pu, H.F.; Zhou, Q.F.; Zhang, Q. Transparent p-type conducting K-doped NiO films deposited by pulsed plasma deposition. *Thin Solid Films* **2012**, *520*, 5884–5888.

[13] Anna Liguori, Chiara Gualandi, Maria Letizia Focarete, Fabio Biscarini and Michele Bianchi, “The Pulsed Electron Deposition Technique for Biomedical Applications: A Review”, Coatings 2020, 10, 16; doi:10.3390/coatings10010016

[14] Massimo Mazzer, Stefano Rampino, Enos Gombia, Matteo Bronzoni, Francesco Bissoli, Francesco Pattini, Marco Calicchio, Aldo Kingma, Filippo Annoni, Davide Calestani, Nicholas Cavallari, Vimalkumar Thottapurath Vijayan, Mauro Lomascolo, Arianna Cretì and

[15] Edmondo Gilioli, "Progress on Low-Temperature Pulsed Electron Deposition of CuInGaSe2 Solar Cells" Energies 2016, 9, 207; doi:10.3390/en9030207

[16] Tommaso Addabbo, Mara Bruzzi, Ada Fort, Marco Mugnaini and Valerio Vignoli, "Gas Sensing Properties of In2O3 Nano-Films Obtained by Low Temperature Pulsed Electron Deposition Technique on Alumina Substrates" Sensors 2018, 18, 4410; doi:10.3390/ s18124410

[17] Agata Niemczyk, Dariusz Moszy´ nski, Roman J¸edrzejewski , Konrad Kwiatkowski, Joanna Piwowarczyk 1 and Jolanta Baranowska, "Chemical Structure of EVA Films Obtained by Pulsed Electron Beam and Pulse Laser Ablation", Polymers 2019, 11, 1419; doi:10.3390/polym11091419

[18] A.Gambardella, M.Berni , G.Graziani, A.Kovtun, A.Liscio, A.Russo, A.Visani, and M.Bianchi, "Nanostructured Ag thin films deposited by pulsed electron ablation", Applied Surface Science Volume 475, 1 May 2019, Pages 917-925

[19] F. Pattini, M. Bronzoni, F. Mezzadri, F. Bissoli,

[20]E. Gilioli and S. Rampino, 2013, "Dynamics of evaporation from CuGaSe2 targets in pulsed electron deposition technique", J. Phys. D: Appl. Phys., vol. 46, p. 245101.

[21 M. Nistor, N. B. Mandache and J. Perriere, 2008, "Pulsed electron beam deposition of oxide thin films", J. Phys. D: Appl. Phys., vol

[22] G. E. Ozur, S. A. Popov, V. F. Fedushchak and A. V. Saushkin, ,2006 ,"Generation of high-intensity pulsed low-energy electron beams in a channel spark system", Technical Physics Letters, vol. 32, pp. 928-931.

[23] Ristein, J., R. T. Stief, L. Ley, and W. Beyer, 1998, "A comparative analysis of a-C: H by infrared spectroscopy and mass selected thermal effusion", Journal of Applied Physics 84, no. 7 .

[24] M. St. C. Flett, Elsevier Monographs: , 1963 ,"Characteristic Frequencies of Chemical Groups in the Infra-Red" ,Elsevier, Amsterdam,.

[25] C. N. R. Rao, 1963, "Chemical Applications of Infrared Spectroscopy", Academic, Boston.

تأثير نوع الغاز على ديناميكيات نظام ترسيب الإلكترون النبضي لقناة الشرارة

صفوت حسب الله[1،2], اسامة راشد [2], احمد صبحى[3] ,محمود الجارحى[4] ,احمد شعبان[5].

[1] قسم الفيزياء ,كلية العلوم ,الجامعة الاسلامية المدينة المنورة,السعودية .
[2] قسم الفيزياء ,كلية العلوم (بنين) جامعة الازهر ,القاهرة ,مصر .
[3] قسم الاطياف ,شعبة الفيزياء ,المركز القومى للبحوث ,الجيزة ,مصر .
[4] قسم الهندسة النووية ,جامعة سول ,سول ,كوريا الجنوبية .
[5] طالب ماجستير قسم الفيزياء ,كلية العلوم (بنين) , جامعة الازهر ,القاهرة ,مصر .

الملخص العربي

في هذا البحث تم دراسة تأثير نوع الغاز على ديناميكيات نظام ترسيب الإلكترون النبضي لقناة الشرارة. تم قياس الخصائص الكهربائية والمغناطيسية للنظام لغازات مختلفة - الأكسجين (O2) والنيتروجين (N2) والأرجون (Ar). تم قياس تيار التفريغ لكل نوع من أنواع الغاز بقيمة قصوى تبلغ 1189 أمبير في حالة O2 عند الجهد المطبق -13 كيلو فولت. تمت محاكاة أشكال موجة التيار والجهد بواسطة نموذج دوائر LRC. كما تم دراسة تأثير ضغط الغاز على تيار التفريغ والحث الكلي. تم قياس تيار شعاع الإلكترون بواسطة faraday cup - أقصى تيار شعاع إلكتروني يبلغ 136 أمبير في حالة غاز O2. تم استخدام ملفي التقاط مغناطيسي لقياسات الديناميات الحركية للحزمة وكانت سرعة الحزمة المقاسة حوالي 0.4 × 10^6 م / ثانية. تم حساب كثافة البلازما لشعاع الإلكترون من faraday cupوإشارات الملفات المغناطيسية ووجدت أنها 1.96 × 10^{20} م$^{-3}$. تم قياس أطياف الانبعاث الضوئي أيضًا لتحديد الذرات والجزيئات النشطة ودورها في تفاعل شعاع الإلكترون مع هدف من الجرافيت لتطبيق ترسيب الأغشية الرقيقة. تم إثبات قدرة استخدام النظام لترسيب الأغشية الرقيقة من خلال ترسيب أغشية الكربون المهدرج غير المتبلور (a-C: H) فوق ركائز السيليكون.